Two-dimensional position measurement using magnetoquasistatic fields

D. D. Arumugam* J. D. Griffin† D. D. Stancil‡ D. S. Ricketts§

Abstract — **Two-dimensional (2-D) measurements of the magnetoquasistatic fields generated from a magnetic dipole (an electrically small current loop) located above the earth are compared to calculations using complex image theory. The magnetoquasistatic coupling between a vertical (i.e., surface normal parallel to the earth) emitting loop and seven vertical receiving loops was measured in a two-dimensional x-y grid of 27.43 m by 27.43 m, all above the earth, where the receiving loops were located outside this grid. Inverting the theoretical expressions to estimate two-dimensional position from measured field values resulted in an average geometric position error of 1.08 m (100^{th} percentile of the measured grid), and an average error of 0.89 m for 95^{th} percentile of measured grid.**

1 INTRODUCTION

Radio position tracking, or position sensing, plays an important, enabling role in society today, especially in applications such as navigation, asset-tracking, and location-based services [1]. While numerous advances have been made, existing systems such as ultra-wideband (UWB), global positioning (GPS), and radio-frequency identification (RFID) systems perform poorly in non-line-of sight (NLoS) environments [2]. Furthermore, because they use propagating electromagnetic waves, these techniques suffer from multipath effects and when used in proximity to weakly conducting dielectric bodies.

We recently introduced a long distance position measurement technique that overcomes these problems by using magnetoquasistatic fields [3]. The technique determines the distance between an emitting and receiving loop by measuring the magnitude of an emitted magnetoquasistatic field at the receiver. Quasistatic magnetic fields are not significantly perturbed by weakly conducting dielectric bodies, and have been used to solve for the position and orientation of an emitting loop at short distances (less than 4-5 m) from a receiver [4]. However, in [3] we showed that, to accurately measure position at long distances, it is necessary to consider not only the primary fields emitted, but also the secondary fields generated by induced currents in the earth. We do this by applying complex image theory [5] to account for the secondary fields. By inverting the theoretical expressions for the coupling

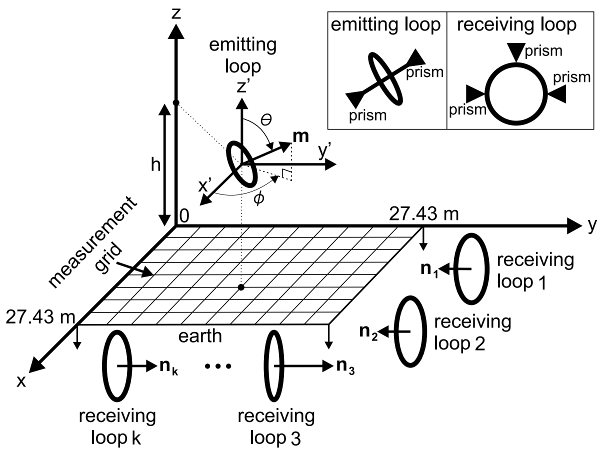

Figure 1: Coupling between an emitting loop and k receiving loops.

between an emitting and receiving loop, we demonstrated, in [3], an accuracy of better than 24 cm for distances up to 34.2 m between one emitter and one receiver (one-dimensional, 1-D) along a direction perpendicular to the surface normal of the loops. For short distances from the emitting loop, the distance estimation error can be significantly reduced by including an accurate expression of the source field [6].

In this paper, we report the extension of our 1-D technique to the 2-D domain, which requires multiple receivers instead of a single receiver. To determine the 2-D location, we measure the magnetic induction generated from a single emitting loop in multiple receiving loops located outside a measurement grid, all above the earth as depicted in Fig. 1. In Section 2, we review our positioning technique and complex image theory. In Section 3, we provide a description and the result of the experiment. Section 4 presents a conclusion.

2 COMPLEX IMAGE THEORY & POSITION MEASUREMENT

We begin by briefly reviewing the main concepts of position estimation using complex image theory to lay the foundation for our measurements [3]. Within the quasistatic region, the fields generated by an arbitrary source at a height $z = h$ above the earth are a function of the source, and its image at a complex depth $z = -h-\delta(1-j)$ beneath the earth[1], where $\delta = \sqrt{1/\pi f \mu\sigma}$, f is the oscillation frequency of the source field, μ is the permeability of the earth and σ is the conductivity of the earth [5]. The magnetic field of a magnetic dipole above the earth is [5]

$$\vec{H}_p(x, y, z) \approx \vec{H}^s_p(x, y, z) + c_p\vec{H}^i_p(x, y, z), \quad (1)$$

*Department of Electrical and Computer Engineering, Carnegie Mellon University, and Disney Research Pittsburgh, Pittsburgh, PA, 15213 USA, e-mail: darumugam@cmu.edu.

†Disney Research Pittsburgh, Pittsburgh, PA, 15213 USA, e-mail: joshdgriffin@disneyresearch.com.

‡Department of Electrical and Computer Engineering, North Carolina State University, Raleigh, NC, 27695, and Disney Research Pittsburgh, Pittsburgh, PA, 15213 USA, e-mail: ddstancil@ncsu.edu.

§Department of Electrical and Computer Engineering, Carnegie Mellon University, Pittsburgh, PA, 15213 USA, e-mail: ricketts@ece.cmu.edu.

[1] Placing an image at a complex depth $z = -h - \delta(1 - j)$ beneath the earth provides a good approximation to the exact formulation of the fields above the earth [5].

where the first and second terms are the fields of the source and complex image, respectively. The subscript $p = ||, \perp$ indicates the components parallel and perpendicular to the ground, respectively; the superscripts s and i indicate the source and the complex image, respectively; and $c_{||} = 1$ and $c_{\perp} = -1$. The magnetic fields of the source and complex image are $\vec{H}^s(x, y, z) = \vec{H}^d(x, y, z - h)$ and $\vec{H}^i(x, y, z) = \vec{H}^d(x, y, -z - h - \delta(1 - j))$, where $\vec{H}^d(x, y, z)$ is the magnetic field of a magnetic dipole at the origin expressed in Cartesian coordinates. It is given by

$$\vec{H}^d(x, y, z) = \frac{1}{4\pi}\left[\frac{3\vec{r}(\vec{m}\cdot\vec{r}) - \vec{m}r^2}{r^5}\right], \tag{2}$$

where $\vec{m}$ is the moment of the magnetic dipole and $\vec{r} = r\hat{r}$ is the position vector from the origin to the point of observation. From Faraday's law, the voltage generated at the terminals of the receiving loop is [3]

$$V = -j\omega\mu_o\left[\hat{n}\cdot\left(\vec{H}_{||} + \vec{H}_{\perp}\right)\right]a, \tag{3}$$

where $\omega = 2\pi f$, $\hat{n}$ is the unit vector of the receiving loop's surface normal, and a is the surface area of the receiving loop.

To solve for the x-y coordinate (two unknowns) of the emitting loop, one must use a minimum of $k \geq 2$ unique equations (diversely located receivers), know a priori the z coordinate, and the orientation of the emitting loop. We seek to minimize the error between the theoretical voltage of (3), V_l^T, and the measured voltage at the terminals of the receiving loop, V_l^M, where $l = 1, \ldots, k$ denote each receiving loop. For $k > 2$, the system is overconstrained, and an optimal solution can be found using a numerical non-linear, least-square optimization algorithm to minimize

$$\Phi = \sum_{l=1}^{k}\left[V_l^T - V_l^M\right]^2. \tag{4}$$

3 DESCRIPTION OF EXPERIMENT

The two dimensional experiment measures the voltage at the terminals of multiple, fixed receiving loops, to determine the position of the emitter by minimizing (4) for the coupling between the emitter and all receiving loops.

The emitter is composed of a 50-turn coil driven by a class E oscillator circuit, with power supplied through a 9V battery, as shown in Fig. 2. The design procedure of Kazimierczuk et al. [7] is used to obtain an oscillation frequency and efficiency of 360 kHz and 93%, respectively, with an output power of 0.56 W using the following component values: $R_1 = 100\ k\Omega$, $R_2 = 51\ k\Omega$, $L_1 = 10\ \mu H$, $L_2 = 120\ \mu H$, $L_3 = 79\ \mu H$, $C_1 = 2200\ pF$, $C_2 = 1500\ pF$, $C_3 = 2.2\ \mu F$, $C_4 = 5600\ pF$, and an STS5NF60L N-CH 60V MOSFET (Q) by ST Microelectronics.

Fig. 3 shows the class E oscillator circuit and 9V battery connected to the terminals of a 50-turn emitting loop [34 American Wire Gauge (AWG) wire]. The loop is coiled around a hollow, RF transparent Delryn/Acetal (polyoxymethylene) tube with an outer diameter of 16.5 cm.

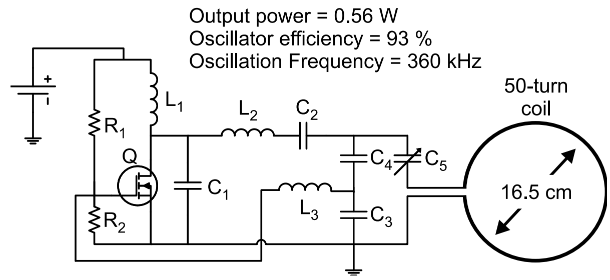

Figure 2: A battery operated class E oscillator circuit.

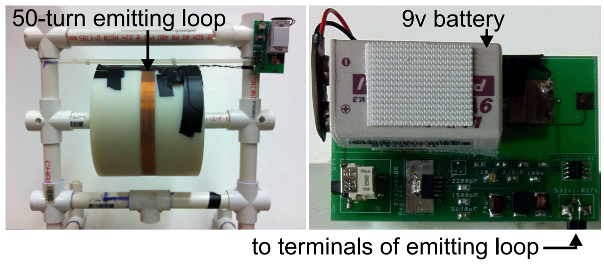

Figure 3: The class E oscillator circuit connected to the 50-turn emitting loop.

The magnetic field of the emitting loop (fed by the class E oscillator) generates a voltage at the terminals of each receiving loop positioned outside the measurement grid (Fig. 1). The RF receiver system used to detect this voltage is shown in Fig. 4. For each receiver system, an active receiving loop with a diameter of 1 m (LFL-1010 by Wellbrook Communications), a band-pass filter to attenuate unwanted signals such as AM broadcast bands and low-frequency maritime radio beacons (bandpass region of 300 kHz to 450 kHz), and an ultra-low-noise amplifier (AD8331 by Analog Devices) is used. The received signals are digitized using a 16-bit 10 MS/s analog-to-digital converter (ADC) included in the PXI-9816D/512 digitizer by Adlink Technologies. A voltage range of ± 1V is used.

The long coaxial cables used to connect the receiving loop antennas, distributed around the measurement field (to the digitizer/ADC), can themselves receive significant signals from the emitter. To reduce the effect of cable coupling, the *loop amplification block* in Fig. 4 is placed directly after the terminals of the receiving loop. This amplifies the signal at the terminals of the receiving loop such that the signal becomes much larger than any signal induced on the long cables, resulting in an improved signal-to-noise plus interference (SNIR) ratio at the ADC. DC power is supplied to the active receiving loop and the *loop amplification block* through a series of bias-tee's shown within both the *RF/DC block* and *loop amplification block* of Fig. 4. The receiver system described in Fig. 4 is repeated for each receiving loop.

Fig. 5a shows the emitter system with the oscillator enclosed within a black thermoplastic [acrylonitrile butadiene styrene (ABS)] box, and the emitting loop covered with an RF transparent foam (C-Foam PF-4 by Cuming Microwave Corporation) for temperature stability (wind/breeze protection). The emitting loop is held by an RF transparent tripod made of Delryn/Acetal (polyoxymethylene). The actual po-

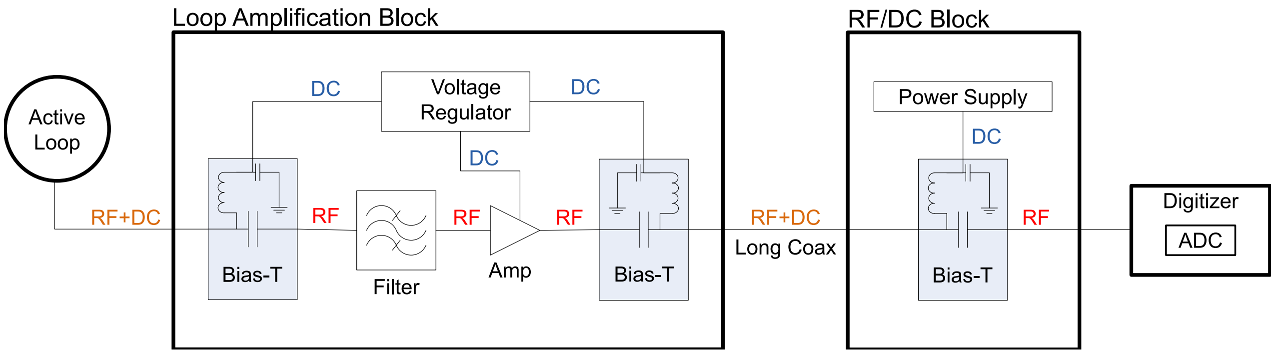

Figure 4: Receiver block diagram with the active receiving loop antenna and RF amplification circuit.

sition of the emitting loop is measured relative to a fixed coordinate using optical surveying instrumentation (CST205 manufactured by CST/Berger) with built-in electronic distance measurements. Two reflective prisms are connected to the emitting loop equidistance from the center and along the surface normal direction of the loop (Fig. 5a and inset of Fig. 1) and are used to measure relative angles and positions of the emitting loop. Fig. 5b shows an active receiving loop (LFL-1010 by Wellbrook Communications) held by a fiberglass surveying tripod (60-FGHD20-BN by CST/Berger). A measurement apparatus containing three reflective prisms are used to measure the relative angles and positions of each receiving loop. The apparatus in Fig. 5b is used only for determining the loop position and orientation, and is removed during RF measurements.

Seven receiving loops (connected to the respective receiver systems) are distributed randomly (positions and orientations) outside a 10×10 measurement grid with an x-y grid spacing of 3.048 m (10 ft). The positions and orientations of the receiving loops, measured using the optical instrument, is plotted on the top-left corner of Fig. 6, where the arrows indicate the direction of the surface normal of the loop. The emitter is moved to each location on the 10×10 measurement grid, and its position and orientation at each location is also plotted on the top-left corner of Fig. 6.

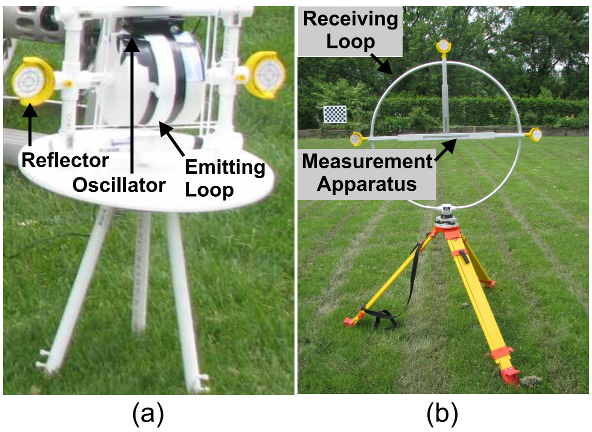

Figure 5: The emitter (a) with an emitting loop connected to the oscillator circuit and two reflectors, and the receiving loop (b) mounted on a tripod and connected to three reflectors. The reflectors are used for position and orientation ground truth measurements.

To study the difference between the theoretically calculated field magnitudes and the measured field magnitudes, the actual positions and orientations of the receiving and emitting loops are used to solve for the voltage using (3) for each of the seven receivers. The results are compared to the measurements at each location of the emitter within the measurement grid. A ground conductivity of $\sigma = 0.055$ S/m, which is within one order of magnitude of previously measured results [8], was chosen to obtain good agreement between the theory and measurements. Fig. 6 (color tiles) shows the absolute value difference of the power in decibels (dB) between the measured results and the voltage solved theoretically [using (3)] (where an impedance of 50 Ω is assumed) using optically measured positions and orientations. The blue (darker-blue) tiles indicate regions within which the difference is approximately one dB (or less), and where higher positioning accuracy is expected.

For the two-dimensional x-y position measurement, the optically measured values of the orientation θ and ϕ, and height z are used to reduce the number of unknowns to three, the x and y coordinate of the center of the emitting loop and σ. We use a value of $\sigma = 0.055$ S/m as before. The estimated two-dimensional position is obtained by minimizing the non-linear objective function in (4) for the voltage measured at the terminals of all seven receiving loops. Fig. 7 (top) shows the estimated position error at each location on the grid obtained through the non-linear minimization, where the optically measured position and orientation of the emitter is used as an initial starting point for the non-linear solver. The figure plots the difference between the estimated location (non-linear solver) and the actual location (optical measurements) in the x-y measurement grid, where the position error is defined as the geometrical distance between the estimated and actual x-y location of the emitter. The results show that an emitting loop can be tracked in a 27.43 m by 27.43 m area with an average error of 1.08 m. Fig. 7 (bottom) shows the average position error as a function of percentiles. For example, the average error for the 100^{th} percentile is calculated using all of the measured grid points while that for the 95th percentile is calculated with 5% of the highest error grid points removed. The 95^{th} percentile has an average error of 0.89 m, and subsequent reduction in error is obtained from lower percentiles.

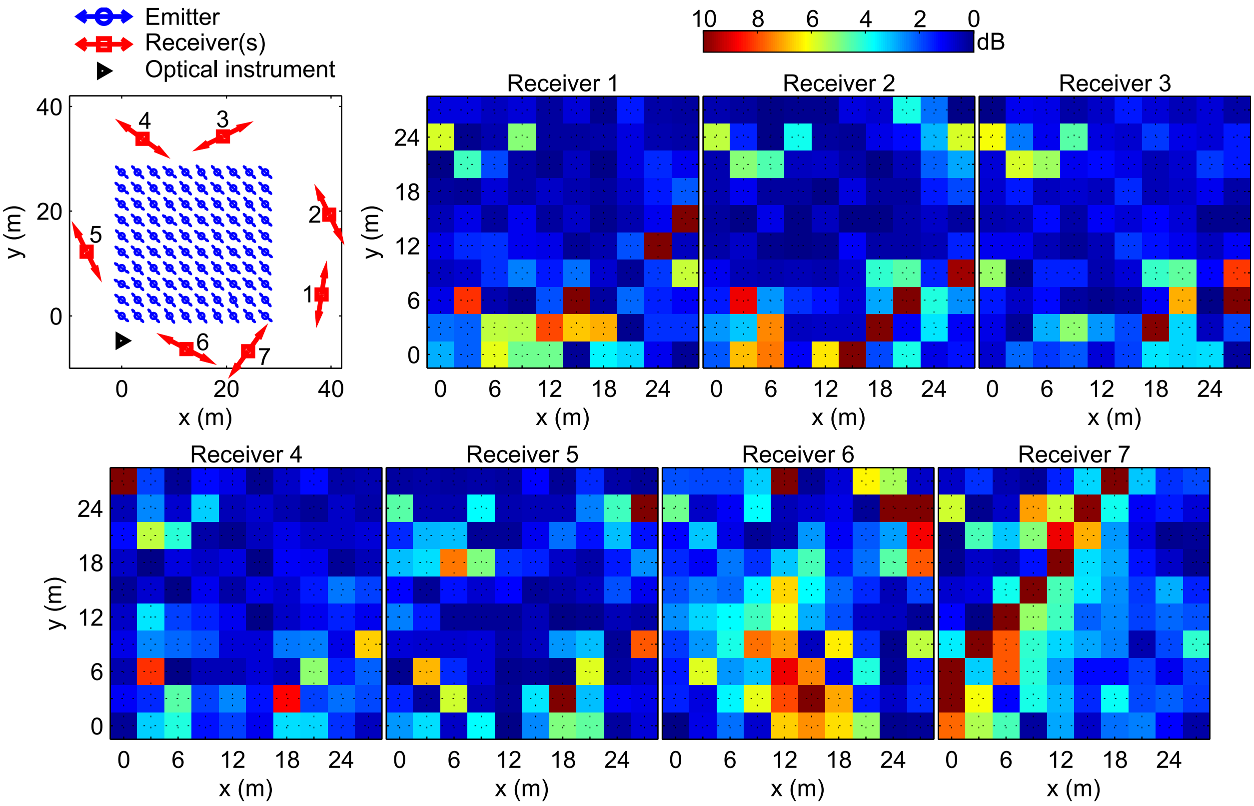

Figure 6: Actual positions and orientations (figure at top-left corner) of the receiving and emitting loops. The arrows indicate the surface normal direction of the loop. The color tiles (the remaining figures) indicate the absolute value difference of the power in decibels (dB) between the measured results and the forward-solved theoretical expressions using optically measured positions and orientations.

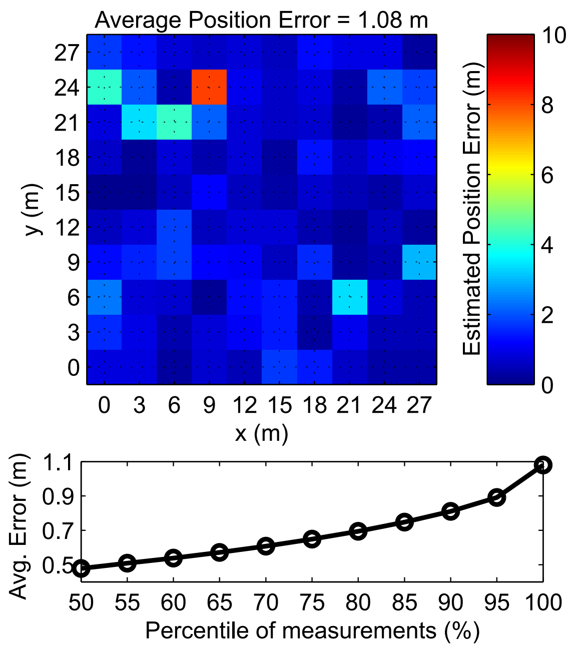

Figure 7: Geometrical distance between the estimated and actual 2-D position.

4 CONCLUSION

In this paper, we extend our 1-D magnetoquasistatic positioning technique in [3] to 2-D and present an experimental demonstration. The results show that an emitting loop can be tracked in a 27.43 m by 27.43 m area with an average error of 1.08 m.

References

[1] H. Liu, H. Darabi, P. Banerjee, and J. Liu, "Survey of Wireless Indoor Positioning Techniques and Systems," IEEE Trans. Sys., Man, and Cybernetics, vol. 37, no. 6, pp. 1067-1080, 2007.

[2] K. Krizman, T. Biedka, and T. Rappaport, "Wireless Position Location: Fundamentals, Implementation Strategies, and Sources of Error," IEEE Vehicular Tech., vol. 47, no. 2, pp. 919-923, 1997.

[3] D. Arumugam, J. Griffin, and D. Stancil, "Experimental Demonstration of Complex Image Theory and Application to Position Measurement," IEEE Antennas Wireless Propag. Lett., vol. 10, pp. 282-285, 2011.

[4] F. Raab, E. Blood, T. Steiner, and H. Jones, "Magnetic Position and Orientation Tracking System," IEEE Trans. on Aero. and Elec. Sys., vol. AES-15, no. 5, pp. 709-718, 1979.

[5] J. Weaver, "Image approximation for an arbitrary quasi-static field in the presence of a conducting half space," Radio Science, vol. 6, no. 6, pp. 647-653, 1971.

[6] D. Arumugam, J. Griffin, D. Stancil, and D. Ricketts, "Higher Order Loop Corrections for Short Range Magnetoquasistatic Position Tracking," IEEE Int. Symp. on Ant. and Prop., accepted.

[7] M.K. Kazimierczuk, V.G. Krizhanovski, J.V. Rassokhina, and D.V. Chernov, "Class-E MOSFET Tuned Power Oscillator Design Procedure," IEEE Trans. on Circuits and Sys., vol. 52, no. 6, pp. 1138-1147, 2005.

[8] H. Fine, "An effective ground conductivity map for continental United States," Proc. IRE, vol. 42, no. 9, pp. 1405-1408, 1954.